Available online at www.sciencedirect.com
ScienceDirect
Trans. Nonferrous Met. Soc. China 25(2015) 3279−3285
Transactions of Nonferrous Metals Society of China
www.tnmsc.cn

Identification and characterization of single crystal $Bi_2Te_{3-x}Se_x$ alloy

Emina POŽEGA[1], Svetlana IVANOV[2], Zoran STEVIĆ[2], Ljiljana KARANOVIĆ[3], Rudolf TOMANEC[3], Lidija GOMIDŽELOVIĆ[1], Ana KOSTOV[1]

1. Mining and Metallurgy Institute Bor, Zeleni bulevar 35, Bor 19210, Serbia;
2. Technical Faculty Bor, University of Belgrade, VJ 12, Bor 19210, Serbia;
3. Faculty of Mining and Geology, University of Belgrade, Đušina 7, Belgrade 11000, Serbia

Received 6 November 2014; accepted 6 April 2015

Abstract: The results of experimental investigation of n-type semiconductor based on Bi_2Te_3 alloy were presented. This material is used in manufacture of thermoelectric coolers and electrical power generation devices. $Bi_2Te_{2.88}Se_{0.12}$ solid solution single crystal has been grown using the Czochralski method. Monitoring of structure changes of the sample was carried out by electron microscope. The elemental composition of the studied alloy was obtained by energy dispersive spectrometry (EDS) analysis and empirical formula of the compound was established. X-ray diffraction analysis confirmed that the $Bi_2Te_{2.88}Se_{0.12}$ sample was a single phase with rhombohedral structure. The behavior upon heating was studied using differential thermal analysis (DTA) technique. Changes in physical and chemical properties of materials were measured as a function of increasing temperature by thermogravimetric analysis (TGA). The lattice parameters values obtained by X-ray powder diffraction analyses of $Bi_2Te_{2.88}Se_{0.12}$ are very similar to Bi_2Te_3 lattice constants, indicating that a small portion of tellurium is replaced with selenium. The obtained values for specific electrical and thermal conductivities are in correlation with available literature data. The Vickers microhardness values are in range between HV 187 and HV 39.02 and decrease with load increasing. It is shown that very complex process of infrared thermography can be applied for characterization of thermoelectric elements and modules.

Key words: Bi_2Te_3; $Bi_2Te_{3-x}Se_x$; single crystal; semiconductor; thermoelectrical properties; hardness; thermovision imaging

1 Introduction

Semiconductors are materials whose electronic properties depend on the energy gap (E_g) width or band gap and dopant concentration. It is well known that semiconductors with a relatively small band gap exhibit very good thermoelectric performance [1−3]. The E_g of semiconductors is relatively small [4] and at the room temperature (300 K) it is 0.66 eV. The energy gap of Bi_2Te_3 single phase varies with temperature and it is 0.13 [5], 0.15 [6,7], 0.21 eV [8] at room temperature.

Tellurium (Te) and selenium (Se) belong to twelve elementary semiconductors. Elementary semiconductors are those in which the properties are dependent on the semiconductor electronic structure. The presence of impurities even in very small proportions can have large effects on the properties of the thermoelectric material [9]. Therefore, the conductivity of semiconductors may easily be modified by introducing dopants into their crystal structure.

The n-type $Bi_2Te_{3-x}Se_x$ semiconductors are well known to have excellent thermoelectric properties near room temperature, and are used in thermoelectric cooling devices and electrical power generation devices. Many studies on these materials have been performed in order to increase the figure of merit, Z, the parameter which evaluates the quality of thermoelectric material [10]. The figure of merit for the undoped Bi_2Te_3 at room temperature is 0.6 [11]. Thermal conductivity can provide information about the temperature range of operation [12]. Typical values of elemental semiconductors for the Seebeck coefficient (S), electrical conductivity (σ), thermal conductivity (λ) and figure of merit (Z_T) at room temperature are: S=200×10^{-6} V·K^{-1}, σ=10^5 Ω^{-1}·m^{-1}, λ=1−100 W·m^{-1}·K^{-1}, Z_T=0.1−1.0, where T is the temperature [13].

The electric conductivity is a characteristic of each material [14]. Only semiconductors offer the right combination of high Seebeck coefficient, high electrical conductivity and low thermal conductivity.

The change in Z_T with temperature for most of the

Corresponding author: Emina POŽEGA; Tel: +381-30-454258; Fax: +381-30-435175; E-mail: emina.pozega@irm.bor.co.rs
DOI: 10.1016/S1003-6326(15)63964-4

known thermoelectric n-type materials studied to date is shown in Fig. 1.

The values of $Bi_2Te_{3-x}Se_x$ alloy for electrical resistivity (ρ), the Seebeck coefficient (S), power factor (F_P) and thermal conductivity (λ) at 250−350 K are: $\rho=10\times10^{-6}$ Ω·m, $S=-200\times10^{-6}$ V·K^{-1}, $F_P=40\times10^{-4}$ W·m^{-1}·K^{-2}, $\lambda=1.4$ W·m^{-1}·K^{-1} [13].

The negative value of the Seebeck coefficient means that the major charge carriers in the sample are electrons.

Bi_2Te_3 has the tetradymite-type rhombohedral structure [14−18]. Bi_2Te_3 melting point is 585 °C [18,19].

The objective of this work is to supplement knowledge of the structure, mechanical and thermoelectrical properties of $Bi_2Te_{3-x}Se_x$ alloy.

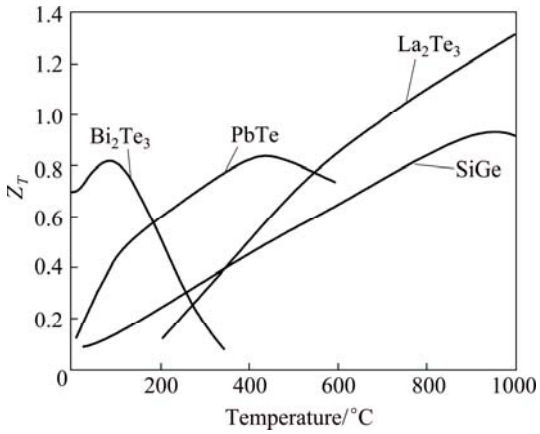

Fig. 1 Value of Z_T for most of known thermoelectric n-type semiconductors [10]

2 Experimental

$Bi_2Te_{2.88}Se_{0.12}$ sample was synthesized using the Czochralski method. Single crystals of 20 mm in length and 8 mm in diameter were obtained by this method. The obtained sample of semiconductor was examined using SEM−EDS, XRD, four probe method for measuring electrical conductivity, Hartman method for measuring specific heat conductivity, DTA, TGA and microhardness measurements. Thermovision imaging was carried out. Structural analysis was done [20] using a Reichert MeF_2 microscope (magnification up to 200) and SEM−EDS. Surfaces of the polished sample for light optical microscopy (LOM) and SEM−EDS prior to metallographic analysis, were etched with hydrofluoric, nitric and acetic acid etching solution to reveal the structure of the investigated sample [21]. EDS analysis was done to determine chemical composition of the studied sample as well as to check sample homogeneity.

The sample was further powdered for XRD analyses. X-ray intensity measurement was carried out on a PHILIPS PW 1710 automated diffractometer using monochromatized Cu K_α radiation (λ=1.54178 Å) and step-scan mode (2θ range was from 4° to 90°, step 0.02°, time 0.5 s). The specific electrical conductivity of the sample d8 mm × 20 mm was measured at 25 °C. Four probe method was used.

The specific thermal conductivity was measured on the same sample and at the same temperature. Harman method was applied.

Phase transition temperatures and the physical property of the sample were analyzed using TG–DTA technique. Differential thermal analysis (DTA) and TG measurements were carried out using SDT Q60 (firm TA instruments) apparatus.

Microhardness was measured using instrument PTM-3 with Vicker's diamond pyramid (Vickers indenter). All the measurements were made at room temperature, and the indentation time was kept at 15 s. Microhardness values vary with load and work-hardening effects of materials. The applied indenter load was varied from 15 to 150 g, and the diagonal of the impression was measured. Hardness of the crystals was calculated using the relation:

$$H_{DP}=1.8544\ P/d^2 \quad (1)$$

where H_{DP} is the Vickers microhardness value; P is the indenter load in kg; and d is the diagonal length of the impression in mm. On each surface, several trials of indentation are taken and the average value of hardness is found.

In these researches, the digital thermal imaging camera Wohler IK 21, whose operation is based on a uncooled germanium thermoelectrical linear detector, has been used.

Thermovision imaging is a non-contact method within real-time register emission of heat or infrared radiation. Since all the bodies emit heat in this way, we can get a clear idea about the temperature of a body in relation to the environment in which the body is. There is almost no area in which this powerful technique is not applied. It is simple to use environmentally and friendly [22,23].

3 Results and discussion

3.1 SEM−EDS analysis

Chemical analysis was done using SEM−EDS giving empirical formula of the compound as $Bi_2Te_{2.88}Se_{0.12}$. SEM image with marked points of EDS chemical analysis of the investigated sample is presented in Fig. 2, while the results of experimental determination of composition by EDS are presented in Table 1.

Figure 2 shows the cracks which appear in the crystal. Special growth conditions are necessary for avoiding these cracks. A low temperature gradient in the

melt and solid is necessary for achieving low dislocation density or strain in the crystal. The role of melt stirring during crystal growth is also crucial.

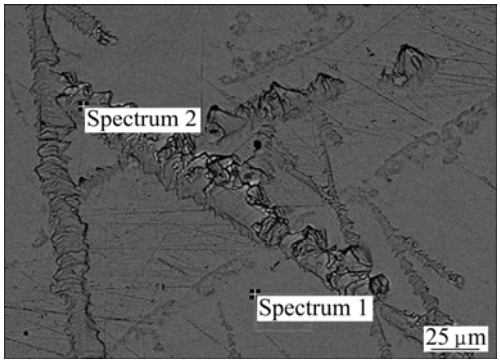

Fig. 2 SEM image (with investigated points) of longitudinal section of $Bi_2Te_{2.88}Se_{0.12}$ sample

Table 1 Results of SEM−EDS analysis of investigated sample $Bi_2Te_{2.88}Se_{0.12}$

Point	Mole fraction/%		
	Bi	Te	Se
Spectrum 1	41.31	56.35	2.34
Spectrum 2	41.10	56.90	2.00

Concentrations of elements in studied points are function of the peak areas in EDS diagram (Fig. 3).

The obtained chemical compositions in the investigated points are similar, which means that the sample has uniform chemical composition (Table 1).

3.2 XRD analysis

Lattice constants of powdered $Bi_2Te_{2.88}Se_{0.12}$ were determined by XRD analysis. The powder XRD patterns of $Bi_2Te_{2.88}Se_{0.12}$ given in Table 2 and Fig. 4, show the presence of only one crystalline phase of a relatively high degree of crystallinity. All reflections in the XRD pattern of $Bi_2Te_{2.88}Se_{0.12}$ were indexed to be a hexagonal unit cell: a=4.368(2), c=30.418(11) Å, V= 502.5(4) Å^3, which is very similar to a=4.3896(2), c= 30.5019(10) Å, V=508.99(4) Å^3 for Bi_2Te_3 [24] and shows that a small portion of Te is replaced with Se. The incorporation of smaller Se leads to the lattice contraction and therefore all diffraction lines were slightly shifted toward bigger 2θ angles with respect to Bi_2Te_3 lines (Fig. 4). Diffraction peaks of basal reflections (specially (0 0 3), (0 0 6) and (0 0 15)) are much more intense than the calculated ones, indicating the existence of preferred orientation due to the layered structure and perfect basal cleavage (Fig. 4).

All semiconductors of the general formula $Bi_2Te_{3-x}Se_x$ are solid solutions, which are isostructural with the Bi_2Te_3. They crystallize in the rhombohedral

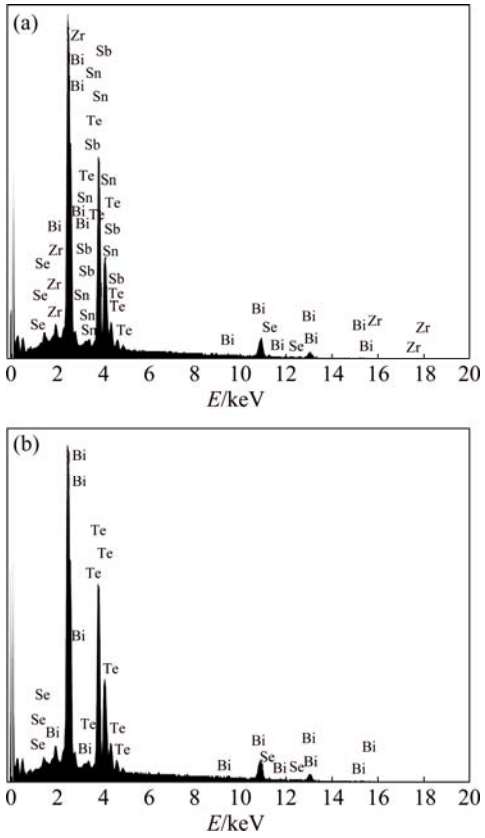

Fig. 3 EDS spectrum 1 (a) and spectrum 2 (b) of $Bi_2Te_{2.88}Se_{0.12}$

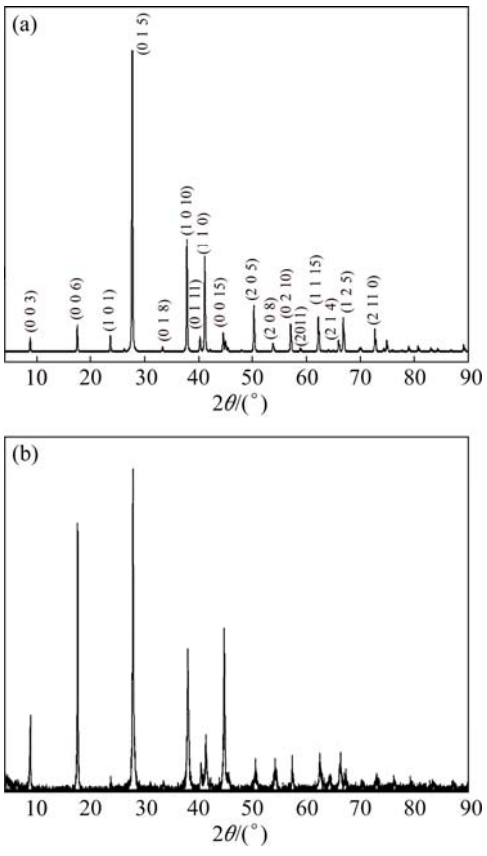

Fig. 4 Calculated XRD pattern of Bi_2Te_3 (a) using structural data given in Ref. [24] and measured powder XRD pattern of $Bi_2Te_{2.88}Se_{0.12}$ (b)

Table 2 XRD powder diffraction data for $Bi_2Te_{2.88}Se_{0.12}$

No.	d/Å	2θ/(°)	(I/I_{max})/%	hkl
1	14.187	6.23	4	–
2	10.063	8.78	25	(0 0 3)
3	5.055	17.53	87	(0 0 6)
4	4.450	19.94	4	–
5	4.126	21.52	4	–
6	3.759	23.65	4	(1 0 1)
7	3.208	27.79	100	(0 1 5)
8	2.883	30.99	4	(1 0 7)
9	2.6755	33.47	4	(0 1 8)
10	2.3708	37.92	43	(1 0 10)
11	2.2311	40.40	7	(0 1 11)
12	2.1843	41.30	11	(1 1 0)
13	2.0268	44.68	48	(0 0 15)
14	1.9901	45.55	4	(1 0 13)
15	1.8065	50.48	7	(2 0 5)
16	1.6927	54.14	6	(2 0 8)
17	1.6079	57.25	7	(0 2 10)
18	1.4866	62.42	9	(1 1 15)
19	1.4482	64.27	4	(0 0 21)
20	1.4137	66.04	7	(0 1 20)
21	1.3911	67.25	5	(1 2 5)
22	1.3392	70.23	4	(1 2 8)
23	1.2960	72.94	4	(2 11 0)
24	1.2503	76.07	4	(0 3 3)
25	1.2068	79.33	4	(1 1 21)
26	1.1567	83.51	4	(1 0 25)
27	1.1279	86.15	4	(0 3 12)
28	1.1185	87.05	4	(0 12 6)

θ—Diffraction angle; d—Interplanar distance; I/I_{max}—Relative intensity; hkl—Miller indices

space group $R\bar{3}m$ (No. 166), and have layered structure of Bi_2Te_3 type. Chalcogens Ha in the structure are placed in two different Wyckoff positions: 3*a* and 6*c*, while the Bi atoms are found in 6*c*. Each chalcogen in the 3*a* position, Ha(3*a*), has 6 neighbouring Bi atoms, while chalcogen in the 6*a* position, Ha(6*c*), has 3 neighbours. This difference in coordination causes different lengths of Ha—Bi bonds: Ha(3*a*)—Bi bonds are longer and Ha(6*c*))—Bi bonds are shorter.

The basic part of the structure consists of five layers —[Ha(3*a*)]—Bi(6*c*)—[Ha(6*c*)]—Bi(6*c*)—[Ha(3*a*)]—. Layers of the Bi and chalcogens are distributed alternately along the hexagonal *c* axis and they are linked by the weak van der Waals bonds.

3.3 Thermoelectric properties

Electrical conductivity σ, Seebeck coefficient S and thermal conductivity λ have been measured to define quality. These properties strongly depend on carrier concentration, mobility, crystal structure and defects in the crystal structure. Values of $Bi_2Te_{2.88}Se_{0.12}$ crystal for electrical conductivity (σ), the Seebeck coefficient (S) and thermal conductivity (λ) at 298 K are: σ=1.03×10^5 S·m^{-1}, S=207×10^{-6} V·K^{-1}, λ=1.77 W·m^{-1}·K^{-1}.

ZHANG at al [25] have investigated 1-D/3-D structured AgNWs/Bi_2Te_3 nanocomposites and found that thermoelectric properties have been dramatically enhanced. Different researches have studied improvement of thermoelectric performance of nanocomposites, too [26−28].

3.4 Differential thermal analysis (DTA)

DTA was carried out under following conditions: air atmosphere, heating rate 10 °C/min, and T_{max}=800 °C. Al_2O_3 was used as a referent material during the measurements. The precision of the measurement in the investigated temperature interval was 2.5 °C. The total mass of the material was 1 g.

Obtained liquidus temperature (613.7 °C) in Fig. 5 is close to melting temperature of Bi_2Te_3 compound, but slightly increased, which can be contributed to the presence of Se. The obtained DTA results imply that the tested material is stable to about 400 °C. The first endothermic reaction at 409.7 °C corresponds to the formation of γ phase (Bi_2Te_2Se) which is affirmed in the studies reported by SOKOLOV et al [29] and LAHALLE et al [30]. The second reaction obtained at temperature of 491.3 °C does not correspond to any phase transformation which may be related to the binary phase diagram of Bi−Te or with phase transformations on Bi−Se binary diagram. We assumed that the second obtained temperature on the DTA curve refers to reaction of two phases: a Bi_2Te_3-based solid solution (β_1) and a Bi_2Te_2Se (γ) [26]. In this work, the range of $Bi_2Te_{3-x}Se_x$ solid solution was determined.

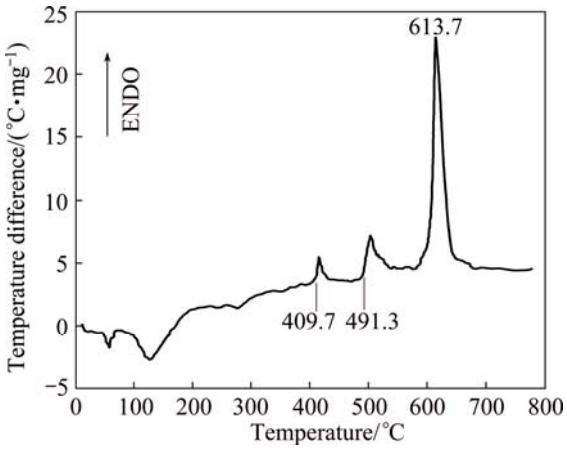

Fig. 5 DTA curve of $Bi_2Te_{2.88}Se_{0.12}$ crystal

TGA was carried out under following conditions: heating rate, 10 °C/min, sample mass 0.182 g, T_{max}= 500 °C in air medium. The curves obtained from thermogravimetric analysis and thermogravimetric (TG) curve show the sample change in mass depending on temperature (Fig. 6). The compound is stable up to 350 °C and, after that, its mass increases which may be due to the undergoing reaction of an intermediate product with nitrogen. This is affirmed in the study reported by DHEEPA et al [31]. HANEMAN [32] has noted that the absorption of gases (O_2, N_2, CO_2) on the obtained bismuth telluride samples is small.

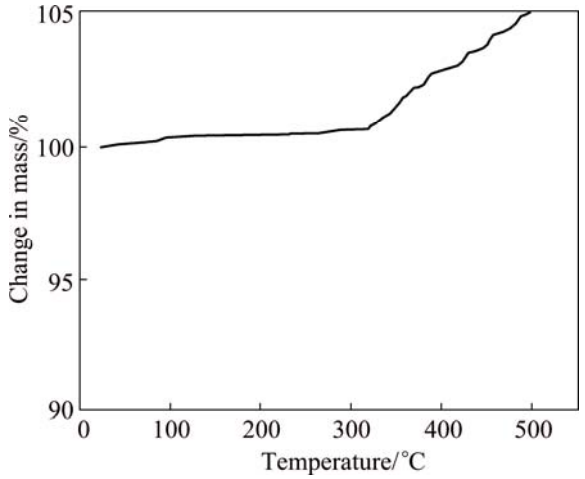

Fig. 6 TG curve of $Bi_2Te_{2.88}Se_{0.12}$ crystal

3.5 Microindentation hardness studies

Structural defects in tested material must affect the results of microhardness measurements. Hardness measurements quantify the resistance of a material to plastic deformation. Microhardness and dislocation density in the case of semiconducting crystals are interrelated.

Table 3 Microhardness of n-type investigated $Bi_2Te_{2.88}Se_{0.12}$ crystal

Load,	H_{DP}					Average value
P/g	1	2	3	4	5	of H_{DP}(HV)
15	75.32	273.7	311.41	194.09	80.51	187
20	149.48	107.35	119.16	80.82	119.16	115.19
30	77.58	99.65	83.36	85.44	52.84	79.77
50	55.28	81.6	68.25	52.03	70.64	65.56
100	57.00	57.00	47.00	43.00		51.00
150	30.53	39.91	46.31	39.31		39.02

Figure 7 shows the variation of hardness with load for bismuth telluride, doped with Se. Hardness decreases with load.

According to literature, undoped single crystals of Bi_2Te_3 have Knoop of 155 N/mm^2 [33]. Since the paper presents different methods of measuring microhardness, the comparative analysis of the obtained results and available literature data is not possible.

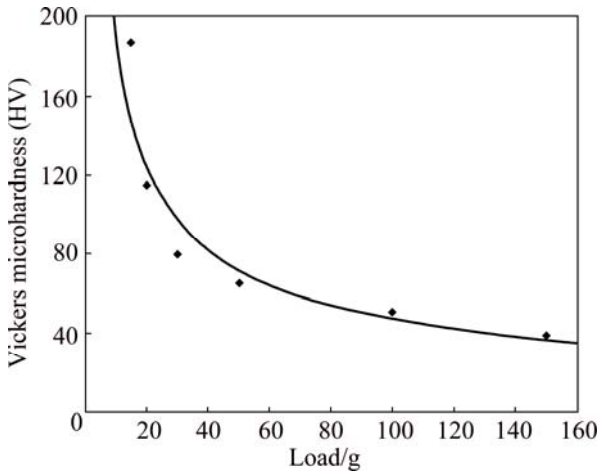

Fig. 7 Variation of microhardness with load for single crystal $Bi_2Te_{2.88}Se_{0.12}$ at room temperature

3.6 Thermovision imaging of TE module

In order to test the efficiency of thermoelectric elements based on Bi_2Te_3 module, 27 elements of the p type measuring of 3 mm × 3 mm × 5 mm and 27 elements of the n type of the same size were developed (Fig. 8). Thermoelectric material of the p-type for the TE modules is $Bi_{0.5}Sb_{1.50}Te_{2.98}Se_{0.02}$ doped with zirconium.

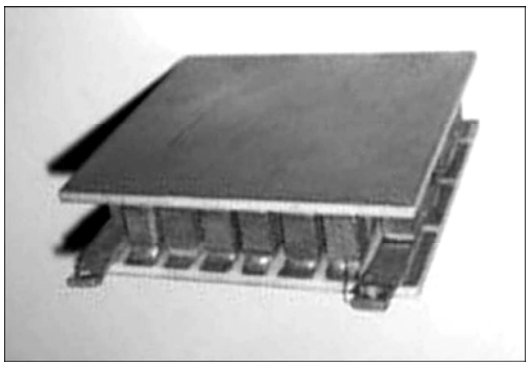

Fig. 8 Thermoelectric module

Thermovision imaging of the module is shown in Fig. 9. One side of the module is heated up to 80 °C and then allowed to naturally cool down. The other side is passively cooled to about 22 °C. The module is loaded by thermogenic consumer of 2.2 Ω resistivity in order to obtain the maximum usable power since in the observing temperature range the internal resistance of the module is approximately constant with amount of 2.2 Ω resistivity. The resulting dependence of the output (electricity) power from the temperature difference at the hot and cold sides is shown in Fig. 10.

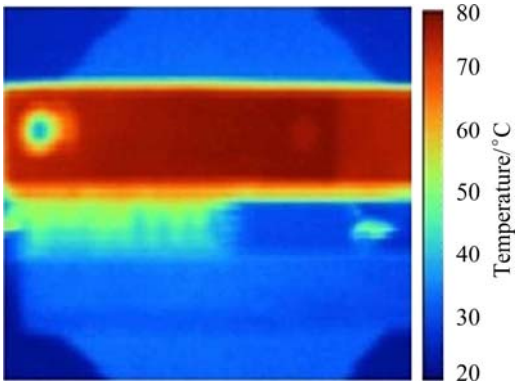

Fig. 9 Thermovision record of thermoelectric module

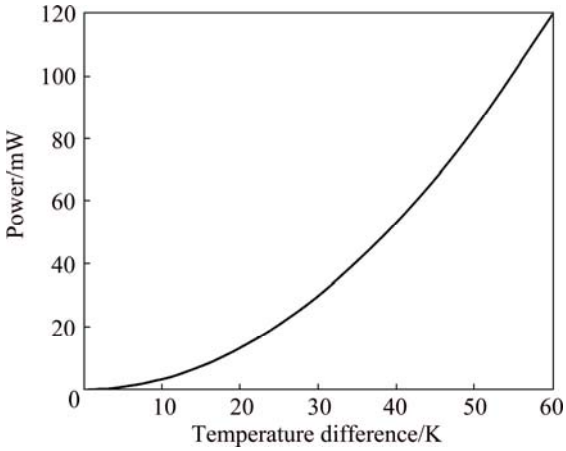

Fig. 10 Dependence of 30 W thermoelectric module output power from temperature difference of hot and cold sides

Figure 10 shows that the temperature difference between the hot and the cold sides is crucial for obtaining significant power at the output of the thermoelectric module.

4 Conclusions

1) A single crystal $Bi_2Te_{2.88}Se_{0.12}$ was investigated using different experimental methods, such as light optical microscopy, SEM−EDS, microhardness analysis, XRD, Four Probe Method, Harman method, TG-DTA and thermovision.

2) EDS analysis was done to determine chemical composition of the studied alloy. The results of the analysis are presented in this work together with the mole ratios of Bi to Te to Se.

3) By methods of differential thermal analysis and X-ray phase analysis, it is proved that the Bi_2Te_3−Bi_2Se_3 section is a system with a continuous series of solid solutions, with the formation of $Bi_2Te_{2.88}Se_{0.12}$ compound below the solidus line. DTA of the material shows the endothermic heat transfer during the process.

4) Microhardness of investigated $Bi_2Te_{2.88}Se_{0.12}$ single crystal alloy in the range of HV 39 to HV 187 is examined using different loads and obtained dependence is presented graphically. In order to test the efficiency of thermoelectric elements based on Bi_2Te_3 module, thermovision imaging is done. It is shown that thermal imaging research can be a simple tool for analyzing the heating uniformity of thermoelectric module.

Acknowledgement

The authors are grateful to the Ministry of Education, Science and Technological Development of the Republic of Serbia for financial support of projects: “Development of ecological knowledge-based advanced materials and technologies for multifunctional application” (Grant No. TR34005) and “New approach to designing materials for energy conversion and storage” (Grant No. OI172060) and “0-3D nanostructures for application in electronics and renewable energy sources: synthesis, characterisation and processing” (Grant No. III45007).

References

[1] POŽEGA E, IVANOV S, STEVIĆ Z, VUKOVIĆ N, GOMIDŽELOVIĆ L, MARKOVIĆ I. SEM−EDS analysis and microindention hardness study of n-type doped BiTeSe alloy single crystals [C]//Proceedings of the 45th International October Conference on Mining and Metallurgy. Bor, Serbia: IRM, 2013: 584−587.

[2] WANG Yi-fu, XIA Qing-lin, PAN Liu-xian, YU Yan. First principles calculation on ternary stannide phase narrow band gap semiconductor Na_2MgSn [J]. Transactions of Nonferrous Metals Society of China, 2014, 24(6): 1853−1858.

[3] NIKOLIĆ P, VUJATOVIĆ S, IVETIĆ T, NIKOLIĆ M, CVETKOVIĆ O, ALEKSIĆ O, BLAGOJEVIĆ V, BRANKOVIĆ G, NIKOLIĆ N. Thermal diffusivity of single crystal $Bi_{0.9}Sb_{0.1}$ [J]. Science of Sintering, 2010, 42: 45−50.

[4] CVEKIĆ V. Semiconductor diodes and transistors [M]. 3rd ed. Beograd: Newspaper−Publishing Company, 1975. (in Serbian)

[5] KAVEI G, KARAMI M A. Thermoelectric crystals $Bi_2Te_{2.88}Se_{0.12}$ undoped and doped by CdC_{l2} or $CdBr_2$ impurities, fabricated and characterized by XRD and Hall effect [J]. Materials Research Bulletin, 2008, 43: 239−243.

[6] TRIPATHI M N, BHANDARI C M. Material parameters for thermoelectric performance [J]. Journal of Physics, 2005, 65(3): 469−479.

[7] HOCHBAUM A I, CHEN R, DELGADO R D, LIANG W, GARNETT E C, NAIARIAN M, MAJUMDAR A, YANG P. Enhanced thermoelectric performance of rough silicon and nanowires [J]. Nature, 2008, 451 (7175): 163−167.

[8] RISTIĆ S. Electronic components [M]. NiŠ: Faculty of Electronic Engineering of Niš, 2011. (in Serbian)

[9] GROVENOR C. Microelectronic materials [M]. Great Britain: Taylor & Francis Group, 1989.

[10] SUMIGA I, GRDJAN M, HUDJEK J. Thermoelectric modules-physical fundamentals and guidelines for use [J]. Technical Bulletin, 2007, 1(1−2): 5−10. (in Serbian)

[11] VUCENOVIĆ M S, SETRAJČIĆ P J. Thermoelectric effect and reuse of heat losses [C]//Renewable Energy Sources and Sustainable Development. Banja Luka: BIH, 2011: 207−214.

[12] BEJENARI M, KANTSER V. Thermoelectric properties of n-type Bi_2Te_3 wires [J]. Moldavian Journal of the Physical Sciences, 2004, 3(1): 94−99.
[13] FLEURIAL P J. Design and discovery of highly efficient thermoelectric materials [2015−03−31]. http://materialsforenergy.typepad.com/files/design-and-discovey-2.p df
[14] MISHRAYZ S K, SATPATHVYZ S, JEPSENZ O. Electronic structure and thermoelectric properties of bismuth telluride and bismuth selenide [J]. Journal of Physics-Condensed Matter, 1997, 9: 461−470.
[15] HONG Soon-jik, CHUN Byong-sun. Microstructure and thermoelectric properties of n-type 95%Bi_2Te_3−5%Bi_2Se_3 alloy produced by rapid solidification and hot extrusion [J]. Materials Research Bulletin, 2003, 38: 599−608.
[16] WIESE J R, MULDAWER L. Latice constants of Bi_2Te_3–Bi_2Se_3 solid solution alloys [J]. Journal of Physics and Chemistry of Solids, 1960, 15(1−2): 13−16.
[17] BOUANANI GHOUMARI H, EDDIKE D, LIAUTARD B, BRUN G. Solid state demixing in Bi_2Se_3–Bi_2Te_3 and Bi_2Se_3–In_2Se_3 phase diagrams [J]. Materials Research Bulletin, 1996, 31(2): 177−187.
[18] GOL'CMAN B M, KUDINOV V A, SMIRNOV I A. Semiconductor thermoelectric materials based on Bi_2Te_3 [M]. 2nd ed. Moskva: Nauka, 1972. (in Russian)
[19] SATTERTWAITE B, URE R. Electrical and thermal properties of Bi_2Te_3 [J]. Physical Review, 1957, 108(5): 1164−1169.
[20] POŽEGA E, IVANOV S, STEVIĆ Z, MARIJANOVIĆ B. Investigation of Bi−Sb−Te−Se−Sn−Zr alloy structure, part I [C]//Proceedings of the 44th International October Conference of Mining and Metallurgy. Bor, Serbia: IRM, 2012: 433−436.
[21] COLIN S, BRANDES E. Metals reference book [M]. 5th ed. London and Boston: Butter Workths, 1976.
[22] STEVIĆ Z, VUJASINOVIĆ M R, ANTIĆ D. Thermal vision application [M]. Bor: University of Belgrade, Technical Faculty Bor. (in Serbian)
[23] POŽEGA E, STEVIĆ Z, IVANOV S, GOMIDŽELOVIĆ L, KRSTIĆ V. Investigation of Bi−Sb−Te−Se−Sn−Zr alloy structure, part II [C]//Proceedings of the 44th International October Conference of Mining and Metallurgy. Bor, Serbia: IRM, 2012: 511−516.
[24] ATUCHIN V V, GAVRILOVA T A, KOKH K A, KURATIEVA N V, PERVUKHINA N V, SUROVTSEV N V. Structural and vibrational properties of PVT grown Bi_2Te_3 microcrystals [J]. Solid State Communications, 2012, 152: 1119−1122.
[25] ZHANG Qi-hao, AI Hin, WANG Wei-jie, WANG Lian-jun, JIANG Wan. Preparation of 1-D/3-D structured AgNWs/Bi_2Te_3 nanocomposites with enhanced thermoelectric properties [J]. Acta Materialia, 2014, 73: 37−47.
[26] ZHANG Qi-hao, AI Xin, WANG Lian-jun, CHANG Yan-xia, LUO Wei, JIANG Wan, CHEN Li-dong. Improved thermoelectic performance of silver nanoparticles-dispersed Bi_2Te_3 composites deriving from hierarchical two-phased heterostructure [J]. Advanced Functional materials, 2015, 25: 966−976.
[27] KIM M Y, YU B K, OH T S. Thermoelectric characteristics of the p-type $(Bi_{0.2}Sb_{0.8})_2Te_3$ nanocomposites processed with SbTe nanowire dispersion [J]. Electronic Materials Letters, 2012, 8: 269−273.
[28] YEE K S, COATES E N, MAJUMDAR A, URBAN J J, SEGALMAN A R. Thermoelectric power factor optimization in PEDOT:PSS tellurium nanowire hybrid composites [J]. Physical Chemistry Chemistry Physics, 2013, 15: 4024−4032.
[29] SOKOLOV O B, SKIPIDAROV S Y A, DUVANKOV N I, SHABUNINA G G. Phase relations and thermoelectric properties of alloys in the Bi_2Te_3−Bi_2Se_3 system [J]. Inorganic Materials, 2007, 43: 8−11.
[30] LAHALLE G C, SCHERRER H, SCHERRER S. Growth of n-type $Bi_2Te_{2.55}Se_{0.45}$ single crystal solid solution by the travelling heater method [J]. Journal of Physics and Chemistry of Solids, 1996, 57: 1713−1717.
[31] DHEEPA J, SATHYAMOORTHY R, VELUMANI S, SUBBARAYAN A, NATARAJAN K, SEBASTIAN P J. Electrical resistivity of thermally evaporated bismuth telluride thin films [J]. Solar Energy & Materials Solar Cells, 2004, 81: 305−312.
[32] HANEMAN D. Adsorption and bonding properties of cleavage surfaces of bismuth telluride [J]. Physical Review, 1960, 119: 567−574.
[33] BERGER L. Semiconductor materials [M]. NW, USA: CRC Press, 1997.

单晶 $Bi_2Te_{3-x}Se_x$ 合金的鉴定与表征

Emina POŽEGA[1], Svetlana IVANOV[2], Zoran STEVIĆ[2], Ljiljana KARANOVIĆ[3], Rudolf TOMANEC[3], Lidija GOMIDŽELOVIĆ[1]

1. Mining and Metallurgy Institute Bor, Zeleni bulevar 35, Bor 19210, Serbia;
2. Technical Faculty Bor, University of Belgrade, VJ 12, Bor 19210, Serbia;
3. Faculty of Mining and Geology, University of Belgrade, Đušina 7, 11000 Belgrade, Serbia

摘　要：研究基于 Bi_2Te_3 合金的 n 型半导体的实验制备。该材料可用于制备热电散热器和发电设备。采用 Czochralski 法制备 $Bi_2Te_{2.88}Se_{0.12}$ 固溶单晶体。采用电子显微镜研究样品的组织变化。利用 EDS 分析实验合金的成分，并确立化合物的经验分子式。XRD 表明 $Bi_2Te_{2.88}Se_{0.12}$ 样品为具有斜方六面体结构的单晶。利用差热分析研究合金的加热行为。利用热重分析研究材料的物理和化学性能随温度的变化。从 XRD 分析得到的 $Bi_2Te_{2.88}Se_{0.12}$ 晶格参数与 Bi_2Te_3 的非常相近，表明只有少部分 Te 被 Se 取代。所得的单晶的比电导率和比热导率与已有数据相符。所得维氏显微硬度为 HV 187~39.02，且随着载荷增加，硬度降低。结果表明可以采用红外热成像法对热电元件和模块进行表征。

关键词：Bi_2Te_3；$Bi_2Te_{3-x}Se_x$；单晶；半导体；热电性能；硬度；热视成像

(Edited by Yun-bin HE)